16th Australasian Fluid Mechanics Conference
Crown Plaza, Gold Coast, Australia
2-7 December 2007

Flow in a Commercial Steel Pipe

R. L. Pepe, M. P. Schultz[1], S. Bailey, M. Hultmark and A. J. Smits

Department of Mechanical and Aerospace Engineering
Princeton University, Princeton, NJ 08544, U. S. A.

[1]Department of Naval Architecture and Ocean Engineering,
United States Naval Academy, Annapolis, MD, U. S. A.

Abstract

Fully-developed turbulent flow in a commercial steel pipe is studied using single component hot-wire probes in both one- and two-point experiments. The streamwise turbulence component was measured over a Reynolds number range from 7.6×10^4 to 8.3×10^6, covering the smooth to fully rough regimes. The experiments were conducted in the Princeton/ONR Superpipe facility that uses compressed air at pressures up to 200 atm as the working fluid. For Reynolds numbers less than about 8×10^5 the surface was hydraulically-smooth, and the results agreed closely with the smooth-wall turbulence intensity and spectral data obtained by Morrison *et al.* [10] and Zhao & Smits [14]. An assessment was performed of probe resolution and results indicate that the turbulence statistics of the large-scale motions were unaffected by the sensing wire length even at high Reynolds numbers. Transitionally-rough and fully-rough data showed deviation from the smooth-wall data as roughness effects became more prominent. In particular, the outer peak in the turbulence intensity observed at high Reynolds numbers in smooth pipe flow decreased in magnitude or stayed constant for transitionally rough and fully rough flow. The two-point azimuthal correlations were found to be consistent with the presence of very large scale coherent regions of low-wavenumber, low-momentum fluid observed in previous studies of wall-bounded flows. The correlations indicated that the azimuthal scale of these regions is Reynolds number independent.

Introduction

Welded commercial steel pipe is probably the most common choice for industrial pipe line applications. It appears, however, that there exist only two laboratory experiments on the behavior of fully-developed flow in commercial steel pipe that cover the smooth, transitionally rough, and fully rough regimes.

The first experiment was that by Bauer and Galavics [2, 3]. Steam at pressures ranging from about 3 to 6 bar was used as the working fluid, and the Reynolds number was varied from 25×10^3 to 2.3×10^6. Three different pipes with diameters of 250, 350, and 450mm were used. The manufacturing processes for the different pipes are not described in detail, and neither are their roughness characteristics, except that Bauer and Galavics [2] report that for the 450mm pipe $k_{rms} = 40\mu$m, so that $k_{rms}/D = 1/2600 = 3.8 \times 10^{-4}$, where k_{rms} is the rms roughness height and D is the pipe diameter. None of these measurements cover the complete transitional roughness region, so that definitive conclusions regarding the transitional roughness behavior cannot be made.

The second experiment was the very recent one by Langelandsvik *et al.* [7]. Mean flow measurements were obtained in a commercial steel pipe with $k_{rms} = 5\mu$m or $k_{rms}/D = 1/26000$, covering the smooth, transitionally rough, and fully rough regimes. This pipe is obviously more representative for a modern steel pipe than the one used by Bauer & Galavics. A scan of the surface is shown in figure 1, and the probability density function of the roughness heights is shown in figure 2. The pdf is bimodal, and well represented by the sum of two Gaussian distributions, each with a standard deviations of 3.2μm, with an offset of about 8μm between them. The friction factor results indicate a transition from smooth to rough flow that is much more abrupt than the Colebrook transitional roughness function suggests (see figure 3). Here, $\lambda = 8u_\tau^2/\langle U \rangle^2$, $u_\tau = \sqrt{\tau_w/\rho}$, τ_w is the wall shear stress, ρ is the fluid density, and $\langle U \rangle$ is the area-averaged velocity. The equivalent sandgrain roughness k_s was found to be 1.6 times the rms roughness height k_{rms}, in sharp contrast to the value of 3.0 to 5.0 that is commonly used. The difference amounts to a reduction in pressure drop for a given flow rate of at least 13% in the fully rough regime. The mean velocity profiles scaled according to Townsend's similarity hypothesis for flow over rough surfaces.

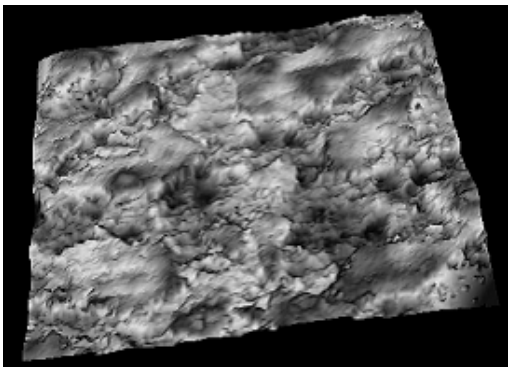

Figure 1: Commercial steel pipe surface scan. From [7].

Here, we report turbulence measurements in the same pipe studied by [7], and they are, as far as we know, the first published data on turbulence in a commercial steel pipe. First, the streamwise turbulence component was measured over a Reynolds number range from 1.5×10^5 to 5.5×10^6, covering the smooth to fully rough regimes, to investigate issues of scaling. Second, two-point hot-wire measurements of streamwise velocity were performed in the logarithmic and wake regions of turbulent pipe flow for Reynolds numbers, based on pipe diameter, ranging from 7.6×10^4 to 8.3×10^6 at four wall-normal positions with azimuthal probe separation. These measurements give some insight into the behavior of the large and very large scale motions.

Experiment

The pipe used in the experiments was 5 in. Schedule 40 welded steel pipe supplied by Lincoln Supply of Trenton, New Jersey. Eight sections of pipe each of length 20 foot were obtained and the inner diameter of each length was measured at six differ-

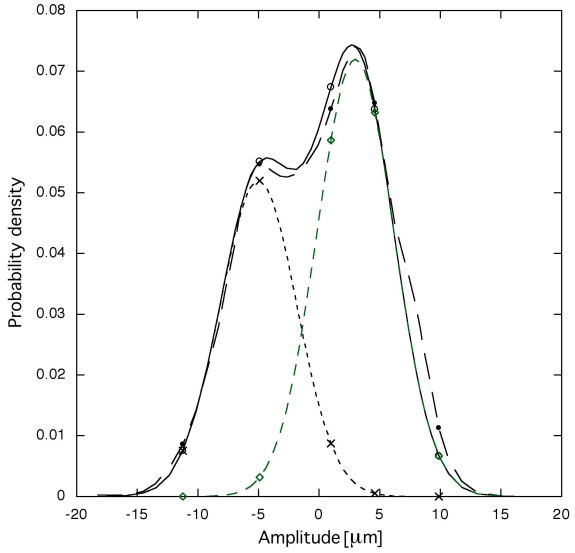

Figure 2: Probability density function of commercial steel pipe roughness. From [7].

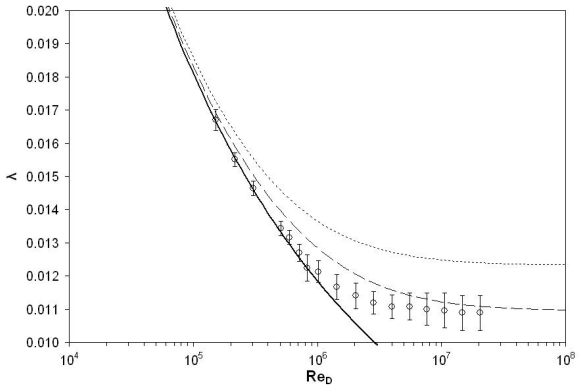

Figure 3: Friction factors for commercial steel pipe. From [7].

ent cross-sections at both ends. These measurements varied between 129.69 mm (5.106 in.) and 130.00 mm (5.118 in) with an average of 129.84 mm (5.112 in.). Each section of pipe had a weld seam about 7-8 mm wide running along its entire length. Near the weld, the pipe was slightly flattened so that the inside diameter decreased by a maximum distance of about 0.4 mm.

The test pipe was installed in the Princeton Superpipe facility (figure 4). The facility uses compressed air as the working fluid to generate a large Reynolds number range, in this case 7.6×10^4 to 8.3×10^6. The facility is described in more detail in reference [13].

Single-Point Measurements

Single-point measurements of the streamwise velocity, $U(t)$, were performed using Dantec compatible normal hot-wire miniature boundary layer probes prepared by Auspex Scientific Corporation. All wires utilized were 2.5 μm diameter. The wire length to diameter ratio varied from about 200 for $Re_D \leq 5.0 \times 10^5$, to about 120 for $Re_D \geq 5.0 \times 10^5$ according to the recommendations by Li *et al.* [8]. The ratios of wire length to viscous length scale ($l^+ = lu_\tau/\nu$) and of wire length to Kolmogorov scale (l/η) can be found in table 1. More detailed information is given by Pepe [11].

Re_D	l [mm]	l/d	l^+	l/η
1.5×10^5	0.50	200	26	8
2.2×10^5	0.50	200	37	10
3.0×10^5	0.45	180	52	11
5.0×10^5	0.50	200	82	18
5.0×10^5	0.30	120	50	11
1.0×10^6	0.30	120	92	17
1.4×10^6	0.30	120	128	22
2.0×10^6	0.30	120	179	28
2.8×10^6	0.30	120	243	35
5.5×10^6	0.33	130	507	62

Table 1: Experimental conditions for single point measurements: Pipe Reynolds number, Re_D, wire length to viscous length, l^+ and wire length to Kolmogorov scale, l/η, at $y/R = 0.1$.

The probe was mounted with the sensing wires normal to the streamwise flow direction on a traversing system which could position the wire within 0.2 *mm* of the wall. This corresponds approximately to $y^+ = 5$ and $y^+ = 200$ for Reynolds numbers of 1.5×10^5 and 5.5×10^6 respectively. The streamwise position of the traversing apparatus was $196D$ downstream of the pipe inlet.

A Dantec Streamline anemometry system was used in constant temperature mode to operate the hot-wire probes. Signals intended for calculating averaged quantities were not filtered and were passed directly to the digitizer. A Krohn-Hite 3988 fourth-order Butterworth filter was used to low-pass filter signals from which spectra were to be calculated. All signals were digitized using 12-bit National Instruments Multifunction DAQ cards (PCI-MIO-16E-4 and PCI-MIO-16E-1). LabVIEW and MATLAB were used for data acquisition.

Measurements of the velocity profile for statistical quantities were sampled at 10 kHz for 30 seconds at 41 wall-normal locations. Each sample was recorded and stored in binary voltage files for each wall-normal location. Convergence studies were performed and found these conditions to be sufficient convergence criteria for the desired statistical quantities for all experiments.

The cut-off frequency was set to 37 kHz for spectral measurements, which were sampled at 75 kHz continuously for 30 minutes at three wall-normal locations.

The hot-wires were calibrated before and after each experiment on the centerline of the pipe. For each calibration, data were sampled at 10 kHz for 30 seconds to obtain converged representations of the mean flow as measured by the Pitot probe and the hot-wire. Measurements of ten to twenty flow velocities were taken to cover the entire range of the experiment. Fourth degree polynomial fits were applied to the calibration data to convert hot-wire voltages to velocities. A number of different Validyne pressure transducers were used in conjunction with the Pitot tube to cover the full range of dynamic pressures encountered in the experiment. A Scanivalve was used to switch among the transducers which covered the ranges of 0.2 *psi*, 1.25 *psi*, 5.0 *psi*, or 12 *psi*.

Two-Point Measurements

Two-point measurements were performed using two single-sensor Dantec compatible hot-wire probes prepared by Auspex

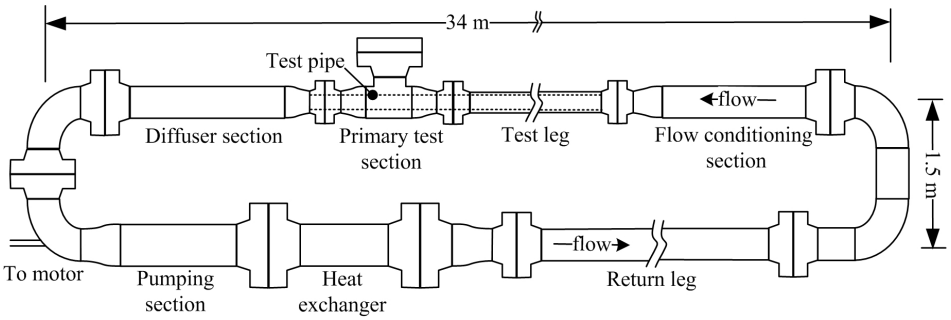

Figure 4: Schematic of the Princeton/ONR Superpipe facility.

Re_D	l [mm]	l/d	l^+	l/η
7.6×10^4	0.50	200	14	5
1.5×10^5	0.50	200	26	7
5.2×10^5	0.50	200	82	18
1.4×10^6	0.50	200	205	35
2.8×10^6	0.50	200	399	58
5.5×10^6	0.50	200	777	95
8.3×10^6	0.50	200	1190	131

Table 2: Experimental conditions for two-point measurements: Pipe Reynolds number, Re_D, wire length to viscous length, l^+ and wire length to Kolmogorov scale, l/η, at $y/R = 0.1$.

Scientific Corporation. The probes were each equipped with platinum plated tungsten wire of 2.5μm diameter and 0.5mm sensing length. The corresponding values of l^+ and l/η are given in table 2. Both probes were mounted onto a custom-designed traversing system at the same streamwise position as the single-point measurements, with the probe sensors aligned in the azimuthal direction. The traversing system was designed such that a single probe could be positioned at a fixed wall-normal location while a second probe at the same distance from the wall could be rotated to an arbitrary angular separation, θ. The second probe was driven at a 1:1 gear ratio by a high resolution (0.45° per step) stepper motor, located outside the test pipe and operated in half-step mode, resulting in an angular resolution of $\pm0.23°$. At the wall-normal positions at which measurements were performed, the corresponding spatial resolution was $1.8\times10^{-3}D$, $1.6\times10^{-3}D$, $1.4\times10^{-3}D$ and $9.8\times10^{-4}D$. The axis system is arranged so that r is the radial direction, y is the wall-normal direction, θ is the angular separation, and $S = r\theta$ is the azimuthal separation distance.

Both probes were operated using the same Dantec Streamline anemometry system used in the single-point study. The anemometer output was sampled at 60kHz and filtered at 30kHz (fourth-order Butterworth filter). The frequency response was always greater than 65kHz. Digitization was performed using a 16-bit simultaneous sample and hold A/D board (National Instruments PCI-6123). Additional digital filtering at 10kHz was performed in post-processing to eliminate electrical noise introduced by the traverse stepper motor. By comparing the data before and after digital filtering, it was concluded that no significant bias was introduced by this additional filtering.

Probe calibration was performed in-situ before and after each measurement run using a Pitot probe located at the pipe centerline. The mean velocity at the probe radial position was determined from the mean centerline velocity using the velocity data from the single-point measurements. Calibration coefficients determined from least-squares fit of King's Law to the calibration data were then used to convert the measured bridge voltages to the effective velocity measured by the probe. This calibration technique yielded second order statistics that agreed to within 10% with values measured during the single-point experiments.

To assess the potential influence of probe blockage and probe interference, we compared the mean and fluctuating velocity components measured by the two probes. Since only one probe was traversed during a measurement run, it is expected that any S dependence of statistics measured by the stationary probe can be attributed to variations in the blockage presented by the traversing apparatus. A slight decrease in the measured mean velocity with increasing S was observed, typically less than 2.5%, consistent with the effects of probe-introduced blockage. The mean-square turbulence intensity was found to be more sensitive, decreasing by as much as 4% with increasing S.

Eccentricity in the traversing probe trajectory is also of concern. It was found that eccentricity caused a difference in the statistics measured by the two probes typically less than 1.5% for the mean velocity and 5% for the mean-square turbulence intensity. The combined blockage and eccentricity errors were determined to be acceptable for the two-point measurements because they did not affect any of our conclusions drawn from these data on the behavior of the for the large-scale structures of interest.

Results

Turbulence Statistics

An important question that arises when measuring turbulence at large Reynolds numbers is whether the measurement volume of the probe is sufficiently small to resolve the turbulent scales of interest. Often the focus is on the near-wall scales where Klewicki and Falco [6] proposed that $l^+ \leq 8$ to resolve the near-wall peak in the streamwise turbulence intensity. It has also been suggested that large-scale statistics can be affected by insufficient measurement volume resolution. As the Reynolds number increases, the question of measurement resolution is increasingly important. For example, in the current study, the ratio of wire length to viscous length scale ($l^+ = lu_\tau/\nu$) varied from 26 to 507 over the full Reynolds number range of the single point measurements (1.5×10^5 to 5.5×10^6). Concurrently, the ratio of wire length to Kolmogorov length (l/η) varied from 8 to 62 over the same range in Reynolds number. This level of resolution is clearly insufficient to resolve, for example, the near-wall peak in turbulence intensity. To investigate the impact of probe resolution on the current experiments, which focus on the large-scale motions, detailed measurements were performed at a $Re_D = 5.0\times10^5$ with wires of sensing length to diameter ratio of $l/d = 200$ and $l/d = 120$. The profiles of mean-

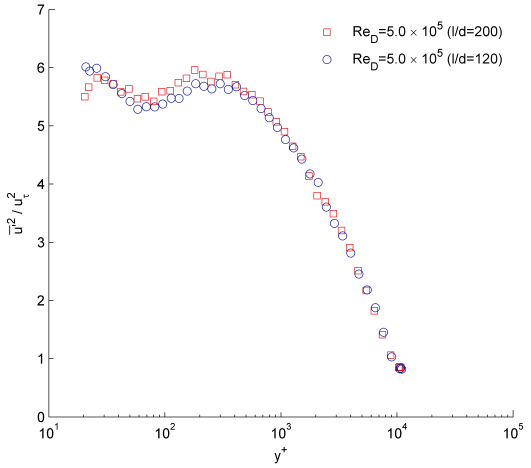

Figure 5: Turbulence intensity profiles at $Re_D = 5.0 \times 10^5$ obtained using two different hot wires with $l^+ = 82$ ($l/\eta = 18$) and $l^+ = 50$ ($l/\eta = 11$), respectively.

squared turbulence intensity, skewness and flatness are shown in figures 5, 6, and 7 respectively. It can be seen that, at this Reynolds number, for moments up to fourth order, the agreement between two probes with spatial resolutions that differ by about a factor of 1.65 is excellent for $y^+ > 50$ ($y/R > 0.005$).

To further assess any possible influence of measurement volume resolution on measurement of large-scale motions in the outer layer, power spectra calculated from single-point and two-point experiment data are shown in figure 8. In this figure the streamwise wavenumber is estimated from $k_x = 2\pi f/\overline{U}$ where f is frequency and $\overline{U}$ is the local mean velocity. Results are shown at $Re_D \approx 5.0 \times 10^5$ for $l^+ = 50$ and 82 (single- and two-point data respectively) and $Re_D \approx 5.5 \times 10^6$ for $l^+ = 507$ and 1190 (two-point data). Spectra are shown at $y/R = 0.1$ so that $y^+ = 1060$ at $Re_D = 5.0 \times 10^5$ and $y^+ = 9980$ at $Re_D = 5.5 \times 10^6$. The spectra were computed using Welch's method with a relatively small Hamming window (2^{11}) and 50% overlap. At both Reynolds numbers the spectra show good overall collapse, indicating satisfactory agreement between single- and two-point data sets and, equally importantly, they show no particular impact of probe resolution. Hence, the spatial resolution of the probes used in this study appears to be adequate to resolve the large-scale motions outside the wall region.

The mean-square turbulence intensities scaled using inner variables over the entire Reynolds number range of single-point measurements are shown in figure 9. A strong Reynolds number dependence is clearly evident, consistent with observations made for smooth pipes by Morrison *et al.* [10] and rough pipes by Allen *et al.* [1]. Two peaks are evident in the profiles of $\overline{u'^2}^+$. The first, at $y^+ \approxeq 25$ is typically associated with the location of peak turbulence production and is discussed in detail in [10]. For Reynolds numbers over 5.0×10^5 a second peak becomes evident in the outer-layer near $y^+ \approxeq 1000$. The magnitude of the peak changes non-monotonically, reaching a maximum value at a Reynolds number of $Re_D = 2.0 \times 10^6$ and then possibly decreasing slightly with further increases in Reynolds number. This observation is in contrast to the smooth-pipe results of [10], which indicate that the peak value continually increases in magnitude with Reynolds number. In the current results the maximum of $\overline{u'^2}^+$ in the outer layer peak occurs at a Reynolds number which corresponds to the onset of transitionally rough flow at $k_s^+ = 1.53$.

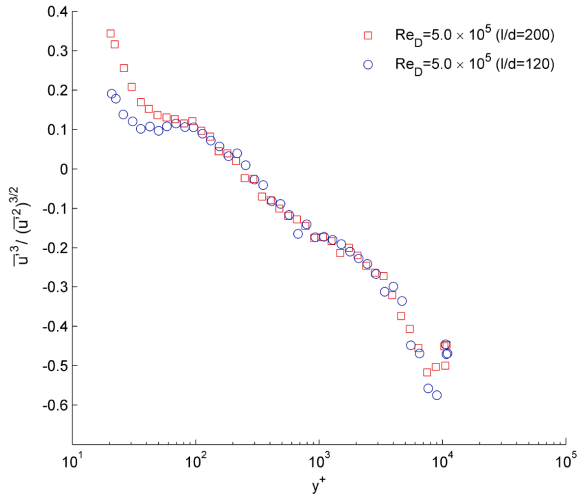

Figure 6: Skewness profiles at $Re_D = 5.0 \times 10^5$ obtained using two different hot wires with $l^+ = 82$ ($l/\eta = 18$) and $l^+ = 50$ ($l/\eta = 11$), respectively.

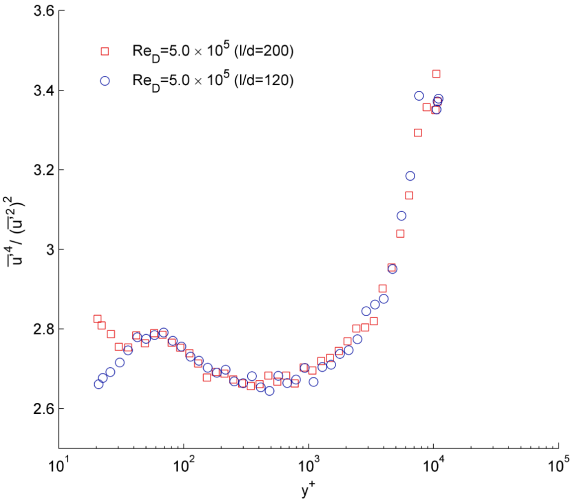

Figure 7: Flatness profiles at $Re_D = 5.0 \times 10^5$ obtained using two different hot wires with $l^+ = 82$ ($l/\eta = 18$) and $l^+ = 50$ ($l/\eta = 11$), respectively.

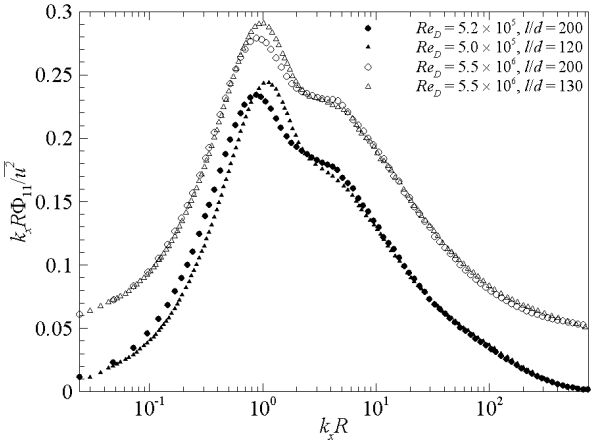

Figure 8: Power spectra at $Re_D \approx 5.0 \times 10^5$ and $Re_D \approx 5.5 \times 10^6$ measured at $y/R = 0.1$ ($y^+ = 1060$ and 9980 respectively) during single-point and two-point experiments using different sensing wire lengths. Spectra at $Re_D \approx 5.5 \times 10^6$ shifted up by 0.05 for clarity.

Figures 10 and 11 show the skewness and flatness profiles, respectively, for all Reynolds numbers tested. When scaled by outer variables, the skewness profiles show no specific effects of either roughness or Reynolds number in the outer region ($0.1 < y/R < 1$) with all test cases showing a decrease in skewness with increasing y/R. Similarly, when the flatness is scaled by outer variables, as shown in figure 11, it appears to be independent of roughness and Reynolds number effects in the outer flow. All cases show that in the outer region the flatness increasees with wall-normal distance.

Correlation Coefficient

Azimuthal profiles of the correlation coefficient were calculated according to

$$R_{uu}(S) = \frac{\overline{u(0,t)u(S,t)}}{\overline{u^2(0,t)}^{\frac{1}{2}}\overline{u^2(S,t)}^{\frac{1}{2}}}, \qquad (1)$$

where the overbar indicates a time average and $u = U - \overline{U}$. The resulting azimuthal profiles of correlation coefficient are presented in figure 12. The profiles are consistent with those previously reported for pipe, channel and boundary layer flows (see, for example, [9] and [4]). Most noticeable is the region of negative correlation occurring in approximately the range $0.3 < S/R < 1.3$, the most likely source of which would be coherent structures in the form of hairpins or counter-rotating streamwise pairs. Such structures have been found to coincide with very-large-scale coherent motions which appear as long, narrow, meandering regions of streamwise velocity deficit that are expected to dominate $R_{uu}(S)$. It is believed that these low momentum regions are induced by the legs of hairpin vortices which have become organized into 'packets'. Streamwise alignment of several of these packets can lead to structures with length an order of magnitude greater than the pipe diameter. Figure 12 shows that the existence of negative $R_{uu}(S)$ occurs for all measured y/R with the greatest magnitude of the negative correlation occurring at wall-normal locations outside the logarithmic layer, suggesting that the importance of these structures is greatest outside the logarithmic layer.

A measure of the azimuthal scale of the coherent structures is the S value at which R_{uu} reaches a minimum, which gives an estimate of the average half-width of the structures. By ex-

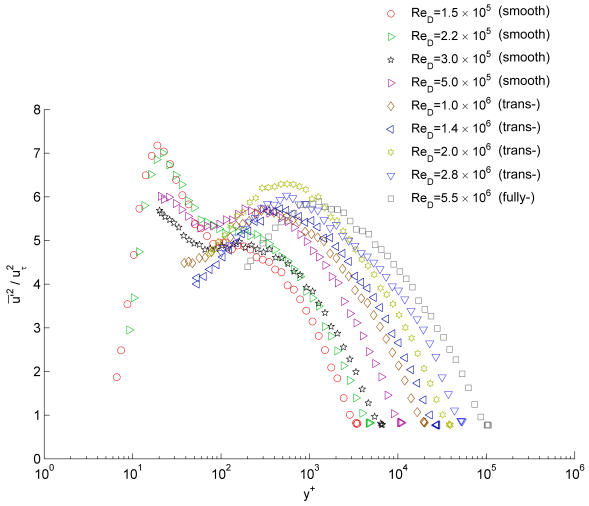

Figure 9: Streamwise turbulence intensity profiles normalized using inner scaling for the full Reynolds number range.

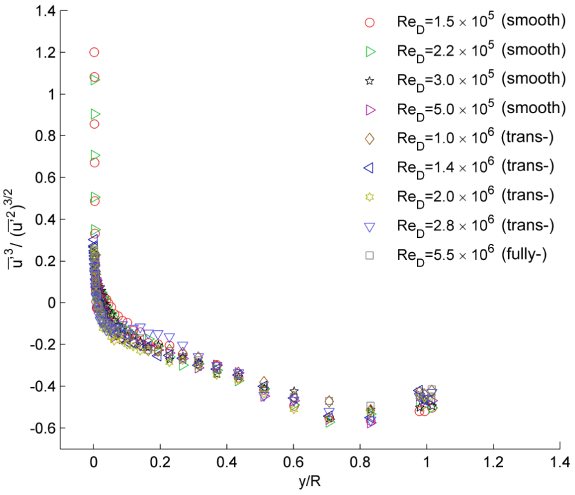

Figure 10: Skewness profiles for the full Reynolds number range.

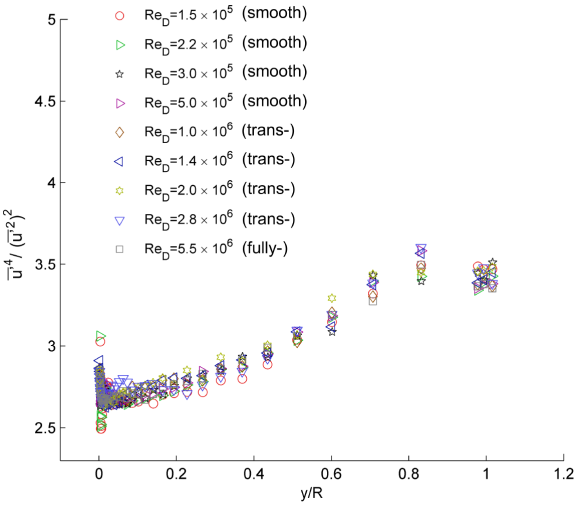

Figure 11: Flatness profiles for the full Reynolds number range.

amining the location of minimum R_{uu}, we find that the structures increase in azimuthal scale as y/R increases, consistent with Townsend's attached eddy hypothesis. A decreasing rate of growth at larger y/R can also be observed in figure 12. In pipe flow, as y/R increases towards unity, the azimuthal scale must approach zero. Hence, this decrease in the growth rate in the outer layer reflects an increase in the influence of pipe geometry on the azimuthal scale of motion.

To illustrate how the very large azimuthal scales under investigation relate to the pipe geometry and to visualize the variation of $R_{uu}(S)$ with wall-normal position, isocontours of $R_{uu}(S)$ are shown in figure 13. This figure further demonstrates the similarity of the azimuthal correlations over a Reynolds number range spanning two orders of magnitude.

Figures 12 and 13 show that the correlations, and therefore the very large-scale motions, show little Reynolds number dependence. This aspect of the VLSM's was previously observed over a smaller Reynolds number range by Hutchins *et al.* [4] in boundary layers and by Monty *et al.* [9] for pipe flows. The results in figures 12 and 13 also indicate that the azimuthal scale of the coherent structures in the outer layer is independent of surface roughness, which is in accordance with expectations based on Townsend's hypothesis.

Conclusions

Single- and two-point velocity measurements were performed over a Re_D range from 7.6×10^4 to 8.3×10^6 spanning hydraulically smooth to fully rough flow in a commercial steel pipe. Through the use of sensing wires of different length at the same flow conditions, it was observed that probe spatial resolution was sufficient to determine accurately the statistics of the large scale motions in the outer layer. Single-point statistics revealed a Reynolds number dependence in the inner-scaled streamwise Reynolds stress. A peak was observed in the outer layer which showed non-monotonic change in magnitude with increasing Re_D, in contrast to smooth pipe data results which increase monotonically. No Reynolds number dependence was observed in the profiles of skewness and flatness in the outer layer. Similarly, the two-point correlations indicated that there was no Reynolds number dependence of the azimuthal scales of motion. These results also indicate that the large-scale motions in the outer layer are independent of surface roughness conditions, consistent with Townsend's hypothesis.

Acknowledgements

This work was supported by the United States Navy Office of Naval Research under Grants N00014-07-1-0111 and N00014-06-WR-2-0346 (Ron Joslin Program Manager). RLP was supported by a National Science Foundation Graduate Research Fellowship. Additional support for SCCB was provided by the Natural Sciences and Engineering Research Council of Canada through the Postdoctoral Fellowship program.

References

[1] Allen, J.J., Shockling, M.A., Kunkel, G.J. and Smits, A.J. Turbulent flow in smooth and rough pipes *Phil. Trans. R. Soc. A.* **365**, 699–714, 2007.

[2] Bauer, B. and Galavics, F. Untersuchungen über die Rohrreibung bei Heiβwasserfernleitungen. *Archiv Waermewirtschaft* **17** (5), 125–126, 1936.

[3] Galavics, F. Die Methode der Rauhigkeitscharakteristik zur Ermittlung der Rohrreibung in geraden Stahlrohr-Fernleitungen. *Schweizer Archiv* **5** (12), 337–354, 1939.

[4] Hutchins, N., Hambleton, W. T. and Marusic, I. Inclined cross-stream stereo particle image velocimetry measurements in turbulent boundary layers. *J. Fluid Mech.* **541**, 21–54, 2005.

[5] Hutchins, N. and Marusic, I. Evidence of very long meandering features in the logarithmic region of turbulent boundary layers. *J. Fluid Mech.* **579**, 1–28, 2007.

[6] Klewicki, J.C. and Falco, R.E. On accurately measuring statistics associated with small-scale structure in turbulent boundary layers using hot-wire probes. *J. Fluid Mech.* **219**, 119–142, 1990.

[7] Langelandsvik, L. I., Kunkel, G. J., and Smits, A. J. Friction factor and mean velocity profiles in a commercial steel pipe. *J. Fluid Mech.*, in press 2007.

[8] Li, J., McKeon, B. J., Jiang, W., Morrison, J. F. and Smits, A. J. The response of hot wires in high Reynolds-number turbulent pipe flow. *Measurement Science and Technology*, **15**, 789–798, 2004.

[9] Monty, J. P., Stewart, J. A., Williams, R. C. and Chong, M.S. Large-scale features in turbulent pipe and channel flows. *J. Fluid Mech*. In press, 2007.

[10] Morrison, J.F., McKeon, B.J., Jiang, W. and Smits, A.J. Scaling of the streamwise velocity component in turbulent pipe flow. *J. Fluid Mech*, **508**, 99–131, 2004.

[11] Pepe, R. V. High Reynolds number turbulence measurements in rough pipe flow. *MSE Dissertation, Princeton University*, 2007.

[12] Schultz, M.P. and Flack, K.A. The rough-wall turbulent boundary layer from the hydraulically smooth to the fully rough regime. *J. Fluid Mech.* **580**, 381–405.

[13] Zagarola, M. V. and Smits, A. J. Mean-flow scaling of turbulent pipe flow. *J. Fluid Mech.* **373**, 33–79, 1998.

[14] Zhao, R. and Smits, A.J. Scaling of the wall-normal turbulence component in high-Reynolds-number pipe flow. *J. Fluid Mech.*, **576**, 457–473, 2007.

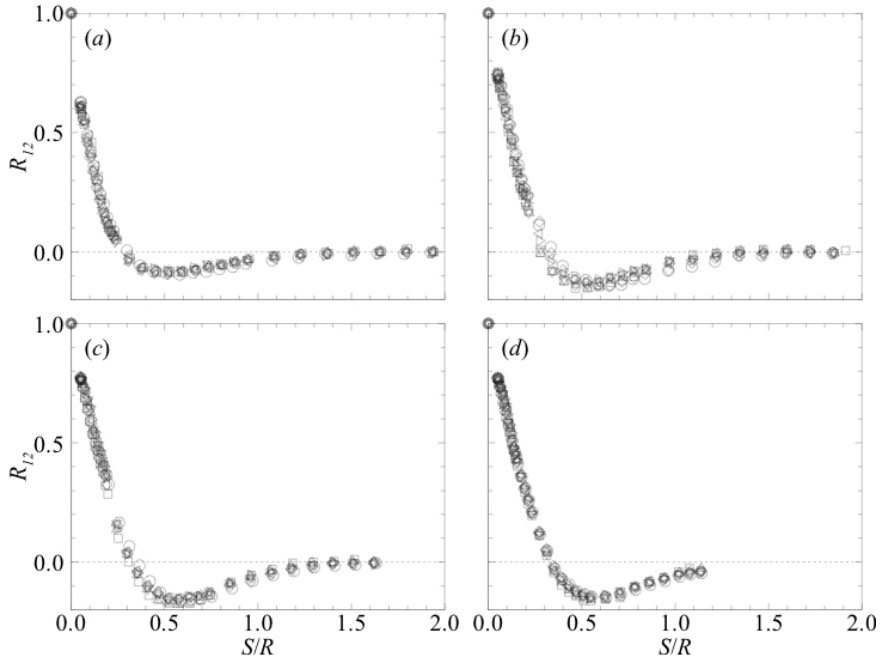

Figure 12: Correlation coefficient measured at (*a*) $y/R = 0.1$, (*b*) $y/R = 0.2$, (*c*) $y/R = 0.3$ and (*d*) $y/R = 0.5$; □, Re_D 7.6×10^4; △, 1.5×10^5; ▽, 5.2×10^5; ▷, 1.4×10^6; ◁, 2.8×10^6; ◇, 5.5×10^6; ○, 8.3×10^6.

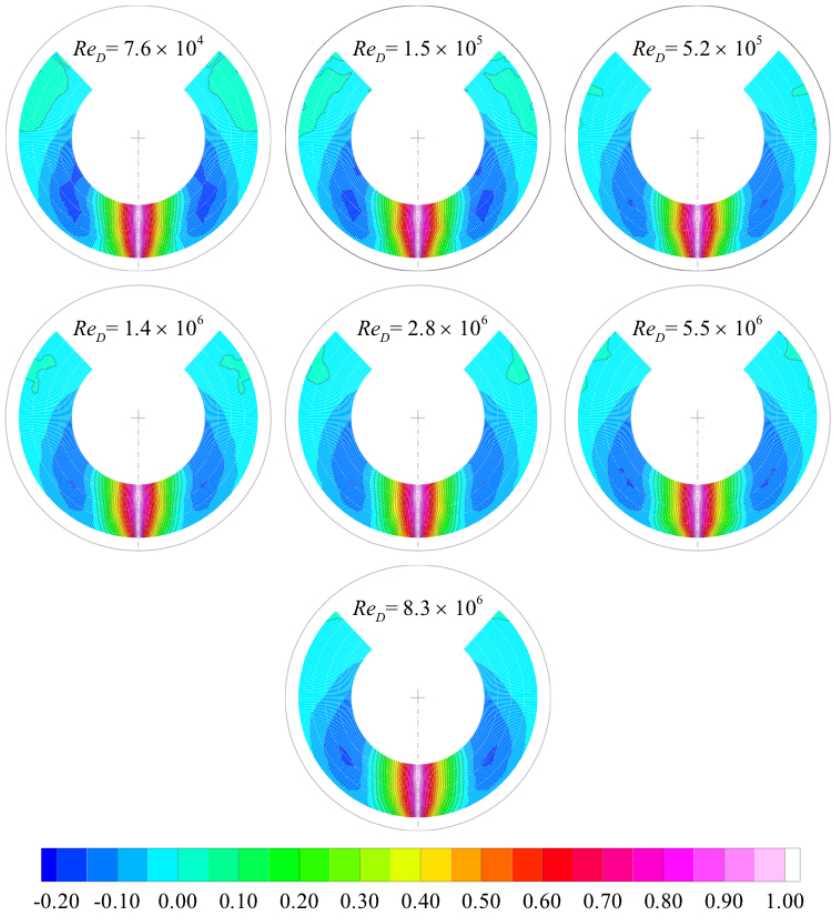

Figure 13: Isocontours of $R_{uu}(S)$ for each Reynolds number investigated. The azimuthal range of the data is expanded by utilizing the even-functioned nature of two-point correlations.